Surface Science 646 (2016) 83–89

Contents lists available at ScienceDirect

Surface Science

journal homepage: www.elsevier.com/locate/susc

Xe adsorption site distributions on Pt(111), Pt(221) and Pt(531)

Andrew J. Gellman *, L. Baker, B.S. Holsclaw

Department of Chemical Engineering, Carnegie Mellon University, Pittsburgh, PA 15213, USA

ARTICLE INFO

Available online 10 November 2015

Keywords:
Pt
PAX
Xe
TPD
Adsorption sites
Chiral

ABSTRACT

The ideal structures of the Pt(111), Pt(221) and Pt(531) surfaces expose adsorption sites that can be qualitatively described as terrace sites on Pt(111), both step and terrace sites on Pt(221), and kink sites on Pt(531). The real surface structures of these surfaces can be complicated by imperfections such as misorientation, reconstruction and thermal roughening, all of which will influence their distributions of adsorption sites. Xe adsorption sites on the Pt(111), Pt(221) and Pt(531) surfaces have been probed using both photoemission of adsorbed Xe (PAX) and temperature programmed desorption (TPD) of Xe. Both PAX and Xe TPD are sensitive to the adsorption sites of the Xe and serve as complementary means of assessing the distributions of adsorption sites on these three Pt surfaces. The adsorption of Xe is sufficiently sensitive to detect the presence of residual steps on the Pt(111) surface at a density of ~1.5% step atoms per Pt atom. On the Pt(221) surface, PAX and Xe TPD reveal adsorption at both terrace and step sites simultaneously. Although the ideal structure of the Pt(531) surface has no well-defined steps or terraces, Xe adsorption indicates that its adsorption sites are best described as a distribution of both step and kink sites with roughly twice as many steps sites as kinks.

1. Introduction

The atomic structure of crystalline metal surfaces is an important determinant of their surface chemistry. For example, molecular adsorption energetics and reaction kinetics on high Miller index metal surfaces with structures exposing step edges can differ greatly from those on the flat low Miller index planes. Enantioselective surface chemistry is an extreme example of structure sensitivity because enantioselectivity can only occur on surfaces with chiral structures that lack mirror symmetry. For metals with face-centered-cubic bulk structures, the naturally chiral surfaces are those that expose kinked step edges [1–3]. It is the local symmetry around the kink sites that imparts chirality and, therefore, the kinks act as chiral sites for enantiospecific adsorption of chiral molecules. Given the Miller indices of a surface, one can readily determine the ideal structure and quantify the areal density of kink sites, step sites and terraces sites. However, the real structures of surfaces are complicated by phenomena such as reconstruction and thermal roughening which invariably cause the site distribution on the real surface to differ from that predicted based on the ideal structure [4–6]. For example, scanning tunneling microscopy (STM) imaging of the chiral Cu(643) surface has shown that the density of kinks is significantly reduced by thermal roughening of the step edges [4,5,7]. Herein, we make use of Xe adsorption as a means of probing the adsorption site distribution on chiral Pt(531) and achiral Pt(111) and Pt(221) surfaces.

Enantiospecific surface chemistry has been studied more extensively on the naturally chiral surfaces of Cu and Pt single crystals than on any other metals. Molecular simulations predicted enantiospecific interactions of chiral hydrocarbons with several naturally chiral Pt surfaces and showed that an understanding of the thermally roughened structures of these surfaces is needed to predict their enantiospecificity [4–6,8–10]. The electro-oxidation of sugars on natural chiral Pt electrode surfaces provided some of the first experimental demonstrations of enantioselective chemistry on naturally chiral metal surfaces [2,3]. Since then, naturally chiral Cu surfaces have been shown to adsorb R-3-methylcyclohexanone enantiospecifically and studies on a variety of different surface orientations have demonstrated that enantioselectivity is very sensitive to the kink structure [11–14]. In the case of Cu(643) surfaces, the real structure has been probed using a combination of STM, photoemission of adsorbed Xe (PAX), and temperature programmed desorption (TPD) of Xe. These have revealed the consequences of thermal roughening on the kink site distribution [7,15]. King et al. have studied the structure of the chiral Pt(531) surface using low energy electron diffraction (LEED) and shown that it is subject to extensive thermal roughening [16,17].

The work described herein uses a combination of PAX and Xe TPD to probe the distributions of adsorption sites on the Pt(111), Pt(221) and Pt(531) surfaces. PAX serves as a probe of adsorption sites simply because the Xe 5*p* binding energies are sensitive to the local work function of the surface on which it is adsorbed and, therefore, differ depending on the structure (terrace, step or kink) or the composition (on an alloy) of the adsorption site [18–20]. Xe TPD can probe adsorption sites, if the Xe adsorption energy is sensitive to the local structure of the adsorption site.

* Corresponding author. Tel.: +1 412 268 3848.
E-mail address: gellman@cmu.edu (A.J. Gellman).

http://dx.doi.org/10.1016/j.susc.2015.10.062
0039-6028/

Xe adsorption on the Pt(111) surface has been studied using a wide variety of experimental and atomistic simulation methods [21–31]. At a coverage of $\theta_{Xe} = 0.33$ Xe/Pt, Xe forms a $(\sqrt{3} \times \sqrt{3})R30$ lattice. The desorption of Xe from Pt(111) at coverages $\theta_{Xe} < 0.33$ reveals zero-order kinetics associated with the existence of an equilibrium between a 2D gas phase and the condensed $(\sqrt{3} \times \sqrt{3})R30$ phase. At coverages $\theta_{Xe} > 0.33$, Xe adopts more complex overlayer lattices in which the Xe atoms are compressed with respect to the $(\sqrt{3} \times \sqrt{3})R30$ lattice. At the onset of the formation of a second layer the coverage is $\theta_{Xe} = 0.41$ Xe/Pt.

Xe adsorption has also been studied on a number of stepped Pt surfaces vicinal to the (111) plane: Pt(332) [32], Pt(997) [24,29,33,34], Pt(11,11,9) [35], Pt(20,20,19) [31]. At very low coverages, Xe adsorbs initially at the step edges, following which it forms islands on the (111) terraces. There is some evidence that the first row of Xe atoms at a step edge is adsorbed on the top of the step [23,28,30]. During heating, desorption from the step edges occurs at higher temperatures than from the terraces. The presence of the steps disrupts the gas–solid equilibrium on the terraces such that desorption from the terraces appears first-order rather than zero-order as on Pt(111) [27,29]. PAX measurements have also been able to observe differences in the $5p_{1/2}$ binding energies of Xe at steps and on terraces on Pt(332) [32] and Pt(20,20,19) [31].

The work described herein has used a complementary combination of PAX and Xe TPD measurements to probe the adsorption site distributions of Xe on the Pt(111), Pt(221) and Pt(531) surfaces (Fig. 1). The Pt(221) surface has (111) terraces separated by straight (110) step edges. Its ideal surface structure has a higher step density than previous studied stepped Pt surfaces and would accommodate one row of Xe atoms at the (110) step edge and only one row on the (111) terraces. The Pt(531) surface is the first kinked Pt surface to be studied by Xe adsorption. Its ideal structure is composed of (111), (110), and (100) microfacets that are one unit cell in width, meaning that Pt(531) does not have any terrace or straight steps wide enough to accommodate a Xe atom that is not adsorbed at the kink. This work uses both PAX and Xe TPD to probe the real structures of these surfaces and the differences from ideality induced by phenomena such as thermal roughening and/or reconstructions.

2. Experimental

The TPD and PAX experiments were performed in an ultrahigh vacuum (UHV) system pumped using stacked turbo-pumps to a base pressure of 5×10^{-11} Torr. Xe TPD and PAX were performed on Pt(111), Pt(221) and Pt(531) surfaces using procedures similar to those reported earlier for similar studies on Cu(111), Cu(221) and Cu(643)^R surfaces [15]. The Pt crystals were mounted to a vacuum sample manipulator through 1 mm Ta wires spot-welded to their edges. The Ta wires were attached to Cu blocks mounted to the cold-head of a closed-cycle Gifford–McMahon cryo-refrigerator (Cryomech AL10). The temperature of the Pt crystals was monitored by means of a type-K thermocouple spot-welded to their edges. The Pt crystals could be cooled to 50 K and resistively heated to >1100 K with the temperature controlled by a computer.

The Pt crystal surfaces were cleaned by cycles of Ar^+ sputtering at an energy of 2500 eV followed by annealing at 1000 K. After introduction of the Pt samples into the UHV chamber, the annealing cycles were conducted in a background of 10^{-6} Torr of O_2 to facilitate the removal of carbon from their surfaces. After sputtering and annealing and prior to performing Xe adsorption, the Pt surfaces were exposed to ~1 Langmuir of O_2 and then heated to observe desorption of CO, CO_2 and O_2 using TPD. The observation of O_2 desorption without any detectable CO or CO_2 was the best means of ensuring that the surfaces were free of carbon contamination.

TPD of Xe was performed using an Extrel quadrupole mass spectrometer. The crystal surfaces were exposed to Xe gas (99.995% UHP from Spectra Gases) by positioning the Pt surface in front of a leak valve fitted with a stainless steel dosing tube. They were then exposed to Xe gas for controlled periods of time at constant pressure. Once Xe was adsorbed, the Pt crystals were positioned in front of the aperture to the mass spectrometer for TPD measurements. A constant heating rate of 0.5 K/s was used in all Xe TPD experiments and the sample temperature was maintained within ±0.3 K of the set-point during heating.

PAX was performed using a Specs 10/35 He(I) photon source and a Specs Phoibos 150 MCD hemispherical electron energy analyzer. The analyzer was operated with an acceptance angle of ±3° and an energy resolution of ΔE < 80 meV. Further reduction of the nominal analyzer energy resolution did not improve the resolution of the PAX spectra as determined from the FWHM of the Xe $5p_{1/2}$ states. In order to obtain PAX spectra at increasing coverages of Xe, the spectra were obtained during adsorption of Xe onto the surface. In other words, a series of spectra were obtained in the presence of a background pressure of ~10^{-9} Torr of Xe while the sample temperature was held at 50 K.

3. Results

3.1. Temperature programmed desorption of Xe from Pt(hkl)

Xe interacts weakly with metal surfaces and desorbs at cryogenic temperatures during heating. On Cu single crystal surfaces, its desorption energetics are only weakly sensitive to surface structure; peak desorption temperatures fall in the range 80 ± 2 K on the Cu(111), Cu(221) and Cu(643) surfaces [15]. Fig. 2 shows Xe TPD spectra obtained from Pt(111), Pt(221) and Pt(531) with initial Xe coverages ranging from θ_{Xe} = ~0.02 to >0.41 Xe/Pt (the saturated monolayer on Pt(111)). The low temperature desorption features at ~60 K are associated with desorption of Xe from a multilayer film and, not surprisingly, show no structure sensitivity. The monolayer coverage of $\theta_{Xe} = 0.41$ is

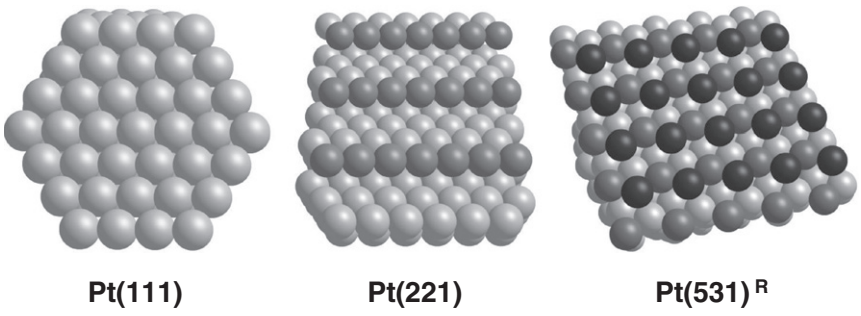

Fig. 1. Ideal structures of Pt(111), Pt(221) and Pt(531)^R. Pt(111) is a close-packed planar surface. Pt(221) contains (111) terraces with (110) type step edges. Pt(531) is a rough, kinked surface with (111), (110) and (100) microfacets that are one unit cell in width. Surface atoms of decreasing coordination are shown with decreasing brightness.

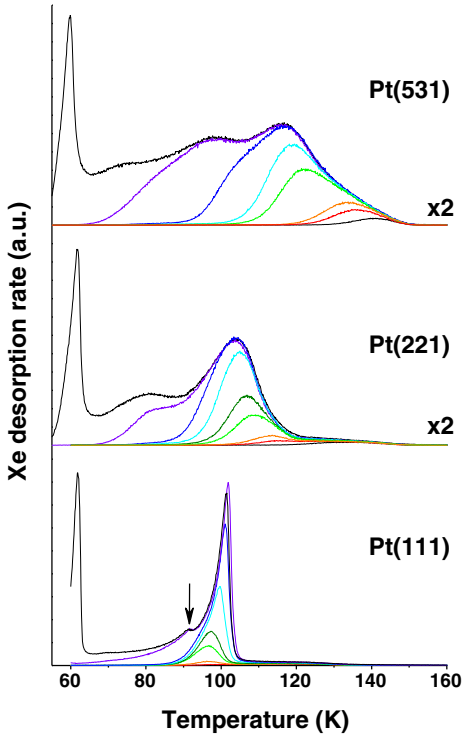

Fig. 2. TPD spectra of Xe on Pt(111), Pt(221) and Pt(531) for initial Xe coverages from ~0.01 to 1 ML. Xe adsorption was performed at <60 K, and the heating rate was 0.5 K/s.

defined, based on prior work on Pt(111) [21,22], as the Xe coverage at which the onset of multilayer desorption is observed and is equated with the area (integrated over T = 65–160 K) under the highest coverage Xe TPD spectrum shown for each surface in Fig. 2. While this definition of coverage is robust for the Pt(111) surface, it should be noted that for Pt(221) and Pt(531), θ_{Xe} is based on the areal density of atoms on the Pt(111) surface rather than the surface atom density of those surface. In other words, in absolute terms a fractional coverage of $\theta_{Xe} = 1$ corresponds to an areal coverage of 1.50×10^{15} Xe atoms cm^{-2}.

In contrast with our prior observations on Cu single crystal surfaces [15], the kinetics of Xe desorption from the Pt single crystal surfaces are structure sensitive. The Xe TPD from Pt(111) shown in Fig. 2 are very consistent with those obtained by Widdra et al. [29]. On Pt(111) the primary Xe desorption feature occurs over a temperature range of 92–105 K and has a shape that is consistent with first-order desorption at low initial coverages transitioning to zero-order desorption as the initial coverage increases and the peak saturates in intensity. This behavior is similar to that on Cu(111) and other close-packed surfaces and arises from a transition from desorption of isolated Xe atoms at low coverage to desorption of Xe from condensed phase islands in equilibrium with a 2D gas [21,25,27,29]. The primary desorption feature at ~100 K is associated with desorption of Xe from a layer with a $(\sqrt{3} \times \sqrt{3})R30$ structure and an absolute coverage of $\theta_{Xe} =$ 0.33 Xe/Pt. At higher coverages, the Xe is compressed into a less stable structure that is incommensurate with the Pt(111) lattice and desorbs from the surface at temperatures down to 62 K, at which point additional Xe adsorbs into the second layer. During TPD with high Xe coverages, there is a clear feature in the desorption rate at 92 K (indicated with an arrow in Fig. 2) that is associated with the transition from the compressed incommensurate layer to the commensurate $(\sqrt{3} \times \sqrt{3})R30$ structure [29]. Finally, to the high temperature side of the primary Xe desorption feature at 100 K, there is a low intensity desorption feature extending from 105 to 135 K and accounting for desorption of Xe at a coverage of $\theta_{Xe} = 0.02$. By comparison with the Xe TPD spectra from Pt(221), Pt(531) and other stepped Pt surfaces [24,27,29] this high temperature shoulder can be attributed to desorption of Xe from residual steps and kinks on the Pt(111) surface.

Xe desorption from the Pt(221) surface is more complicated than from Cu(221) [15]. Desorption from the Cu(221) surface shows a single desorption feature at 78–81 K that transitions with increasing coverage from first-order to pseudo zero-order desorption. On the Pt(221) surface, Xe desorption spans a much wider range of temperatures. At very low initial Xe coverages of $\theta_{Xe} < 0.02$ ML, desorption occurs over a temperature range from 125 to 150 K. By comparison with the TPD data from the Pt(531) surface we attribute this to Xe desorption from kinks in the existing step edges on the Pt(221) surface. At higher initial coverages, the Xe desorption features appear to be first-order but the peak temperatures decrease from 115 to 105 K. The terraces on the ideal Pt(221) surface can only accommodate two rows of Xe atoms. Assuming that the true structure of the surface exposes a distribution of terrace widths, the shift from 115 K to 105 K may simply reflect adsorption at the step edges initially, followed by adsorption in rows that are increasingly further removed from the step edge and increasingly similar to the terrace sites of the Pt(111) surface.

Prior work has studied the adsorption of Xe on the Pt(997) and Pt(11,11,9) surfaces which have a step structure identical to that of Pt(221) but with the terraces separating those steps that are roughly two to three times as wide as those on Pt(221) [24,29,33,35]. On Pt(997), Xe adsorbs first at the step edges and then in a row-by-row manner across the (111) terrace. The (110) step edges on Pt(997) and Pt(221) do not run parallel to the close-packed directions of the $(\sqrt{3} \times \sqrt{3})R30$ structure that forms on the Pt(111) surface and thus, the step edges hinder the formation of such domains on the terraces. The desorption of Xe from both Pt(997) and Pt(11,11,9) surfaces appears to be first-order with respect to its coverage dependence and occurs at temperatures slightly higher than those observed for Xe desorption from Pt(111) [29,33,35,36]. The width of the desorption temperature range from Pt(221) and its shift with coverage reflect the higher step density and higher degree of adsorption site inhomogeneity. At initial coverages of $\theta_{Xe} > 0.33$, Xe desorption from the Pt(221) surface is observed in the temperature range 65–92 K, similar to the case on Pt(111) and suggesting the presence of a compressed monolayer with repulsive interactions between Xe atoms.

The TPD of Xe from Pt(531) shown in Fig. 2 are the only such data from a surface with kinks. These reveal a continuous decrease in the peak desorption temperatures and leading edges as the initial Xe coverage is increased. The peak temperature at lowest initial Xe coverage occurs at ~140 K and must arise from Xe desorbing from kinks on the Pt(531) surface. The continuous distribution of peak desorption temperatures is reflective of an inhomogeneous distribution of adsorption sites that are populated in the order of decreasing adsorption affinity for Xe. The fact that there is Xe desorption over the temperature range 65–95 K also suggests that Xe can adsorb into a high density ($\theta_{Xe} > 0.33$) compressed phase in which there are repulsive interactions between Xe atoms. It is clear from the above that Xe desorption kinetics from the Pt single crystal surfaces exhibit much greater surface structure sensitivity than on Cu surfaces [15]. However, the inhomogeneity of the sites coupled with Xe–Xe interactions complicate the use of these Xe TPD spectra for quantification of adsorption site distributions.

3.2. Photoemission of adsorbed Xe on Pt(hkl)

Although the previously studied desorption of Xe from the Cu single crystal surfaces showed no structure sensitivity, PAX spectra from those surfaces allowed quantitative extraction of adsorption site distributions in terms of terrace, step and kink sites [15]. In this work, PAX was used to gain insight into the adsorption site distributions of Xe on Pt(111), Pt(221) and Pt(531). Ultra-violet photoemission spectra were obtained

from the clean Pt surfaces and then PAX spectra were obtained while continuously exposing the Pt surfaces at 50 K to Xe and, thereby, slowly increasing θ_{Xe}. The raw PAX spectra over the binding energy range 4 to 8 eV are shown in Fig. 3. The spectra from the clean Pt surfaces are shown with dashed black lines. On Pt(111) the Xe $5p_{1/2}$ peak occurs at a binding energy of 6.03 eV and clearly increases in intensity with increasing Xe coverage. The Xe $5p_{3/2}$ feature is clearly split into contributions from the $m_j = \frac{3}{2}$ and $\frac{1}{2}$ levels at binding energies of 4.9 and 4.5 eV. The Pt(221) Xe $5p_{1/2}$ PAX spectra are similar to those obtained from Cu(221) with two dominant peaks that are attributable to adsorption at terrace sites (6.1 eV) and step sites (6.4 eV). Note that these sites appear to fill simultaneously as the coverage increases. Interpretation of the $5p_{1/2}$ PAX spectra from the Pt(531) surface is complicated by the overlap with the high binding energy tail of the $5p_{3/2}$ feature. The $5p_{1/2}$ peak appears to be attributable to a distribution of several types of adsorption sites that would be described as step sites and kink sites.

Subtraction of background signal from the PAX spectra obtained from the Pt surfaces was more complicated than it was for PAX spectra obtained from the Cu surfaces. This arose from the fact that the binding energies on Pt were significantly lower than those on Cu resulting in overlap with photoemission intensity from the Pt valence band. On the Pt(111) surface, the Xe $5p_{1/2}$ level has a binding energy of 6.03 eV, significantly lower than the value of 7.28 eV observed on Cu(111) [15]. As a result, only the $5p_{1/2}$ peaks were used for further analysis, with background subtraction applied only to the range 8.5–5.0 eV. After subtracting the UPS signal from each of the clean surfaces, $I_{hkl}(E;\ \theta = 0)$, from each of the PAX spectra, $I_{hkl}(E;\ \theta)$, a linear background was subtracted. The linear background was unique to each spectrum. The linear backgrounds, $\alpha + \beta E$, were determined by fitting the residual signal, after subtraction of the clean surface spectra, over the binding energy ranges 8.5 to 7.5 eV for Pt(111) and 8.5 to 8.0 eV for Pt(221) and Pt(531). These ranges had no interferences from adsorbed Xe. Eq. (1) summarizes the baseline subtraction process.

$$\bar{I}_{hkl}(E;\theta) = [I_{hkl}(E;\theta) - I_{hkl}(E;0)] - (\alpha + \beta E) \quad (1)$$

The background-subtracted PAX spectra, $\bar{I}_{hkl}(E;\ \theta)$, at various Xe coverages and on all three surfaces are shown as the discrete data points in Fig. 4. The features in the binding energy range 5.75–7.25 eV arise from the Xe $5p_{1/2}$ level and are clearly sensitive to the structure of the Pt surfaces.

4. Discussion

4.1. Quantification of adsorption site distributions from PAX

The Xe TPD and PAX spectra in Figs. 2 and 4, respectively, clearly reveal sensitivity to the structures of the Pt(111), Pt(221) and Pt(531) surfaces (Fig. 1). Our prior study of Xe adsorption on Cu single crystal surfaces revealed similar sensitivity of the PAX spectra to surface structure in spite of the fact that the TPD spectra were comparatively insensitive to surface structure [15]. In that work, the Xe adsorption site density, defined in terms of terrace, step and kinks, was quantified solely on the basis of the PAX spectra. In this work, we have been able to combine both the Xe TPD and PAX spectra in order to quantify Xe adsorption site distributions over the coverage range $\theta_{Xe} = 0$ to 0.33 (or 0.50×10^{15} Xe atoms cm^{-2}).

The background-subtracted PAX spectra, $\bar{I}_{hkl}(E;\ \theta)$, were fit using three pure Lorentzian functions; one for each binding site type. This was the basis for a simple 6-parameter fit used to extract the intensity of each peak from the set of 21 PAX spectra obtained at different coverages on three different Pt surfaces. Like the fit of the PAX spectra obtained from Cu surfaces, the 6 parameters consisted of a binding energy, $E^{site}_{5p1/2}$, and width, $w^{site}_{5p1/2}$, for each of the peaks associated with the three different adsorption sites (terrace, step and kink). In

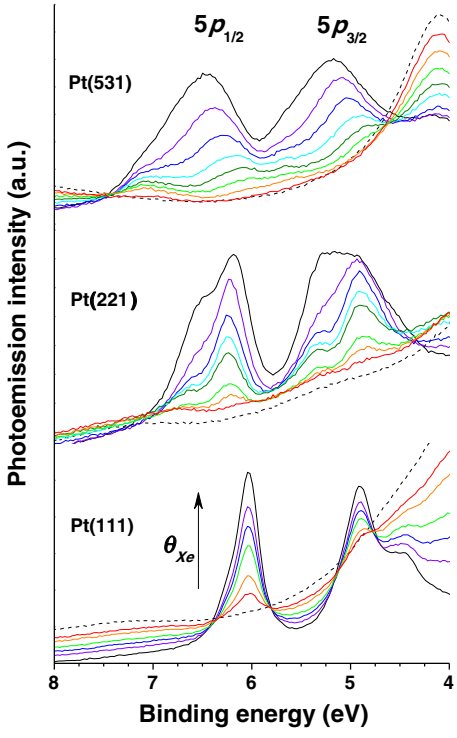

Fig. 3. PAX spectra from Pt(111), Pt(221) and Pt(531) surfaces with Xe coverages in the range <0.1 to 1 ML. Xe adsorbed at step and kink sites on Pt(221) and Pt(531) yield high binding energy features on the $5p_{1/2}$ and $5p_{3/2}$ peaks that do not appear in the PAX spectra from the Pt(111) surface.

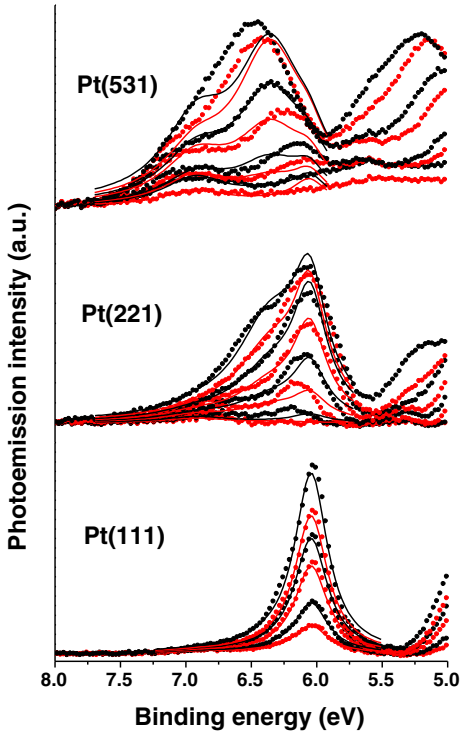

Fig. 4. Fits of the PAX spectra on Pt(111), Pt(221) and Pt(531) surfaces using the peak parameters in Table 1. The symbols are baseline subtracted data points and the solid lines are spectral fits.

Table 1
PAX fitting parameters.

Site	$E_{5p1/2}$ (eV)	$w_{5p1/2}$ (eV)
terrace	6.06	0.31
step	6.36	0.64
kink	6.93	0.59

total, 21 PAX spectra were fit simultaneously: 6 for Pt(111), 7 for Pt(221) and 8 for Pt(531). The 6 fitting parameters were identical for all 21 spectra and independent of surface structure and the Xe coverage. This is the simplest possible fitting scheme. The simple 6 parameter fits to each of the of the baseline-subtracted Pt $5p_{1/2}$ PAX spectra are shown as solid lines in Fig. 4. The fitting parameter values are found in Table 1.

As a caveat, it is important to note that Xe atoms at sites that we might designate as terraces, steps or kinks must experience an inhomogeneous distribution of local work functions in the sense that kinks can be formed by the intersections of steps of various lengths, steps sites are located at various distances from kinks, and terrace sites at various distances from steps. The fact that the PAX peak widths from steps and kinks are greater than the peak width from the Pt(111) terraces, suggests that inhomogeneity is more prevalent for the steps and kink sites than for the terrace sites. This inhomogeneity undoubtedly contributes to the decreasing quality of the fits to the PAX spectra (Fig. 4) as the complexity of the surface structure increases. Realistically, however, we do not feel that we can extract more detailed descriptions of the site types and distributions than by simply classifying them as kinks, steps and terraces.

The intensities associated with each of the three peaks used to fit a given PAX spectrum were dependent on the surface orientation and the Xe coverage. Peak intensities were only allowed to increase or remain constant with increasing Xe coverage, forcing the coverages on each type of site to increase monotonically. The fits at saturation coverage of $\theta_{Xe} = 0.41$ for each surface are shown in Fig. 5. Note that the saturation coverage value of $\theta_{Xe} = 0.41$ is used for all three surfaces, but represents a coverage of 0.41 relative to the areal density of Pt atoms in the Pt(111) surface. The fit to the Pt(111) data at saturation coverage appears to be fairly good. The $5p_{1/2}$ spectra for this surface contain one large peak at $E^{terr}_{5p1/2} = 6.06$ eV from Xe adsorbed at terrace sites and a small, higher binding energy peak at $E^{step}_{5p1/2} = 6.36$ eV from Xe adsorbed at residual steps. However, since the same value of $E^{terr}_{5p1/2}$ was used for all three Pt surfaces, it has been shifted to slightly higher energy than best fits the primary $5p_{1/2}$ PAX peak on the Pt(111) surface. The fit to the Pt(221) PAX spectrum at saturation coverage also appears to be quite good. The fit to the Pt(531) PAX spectrum is not as good as those for the other surfaces. In part, this is the result of overlap of the low binding energy region of the Xe $5p_{1/2}$ feature (terraces sites) with the high binding energy tail of the Xe $5p_{3/2}$ feature (kink sites). This probably renders the PAX-based estimate of the Xe coverage at terraces sites on Pt(531) quite poor. The PAX based estimates of fractional site coverage on each of the Pt surfaces are shown in Fig. 6 by open symbols. These give the fractions of Xe at the terrace, step and kink sites as functions of θ_{Xe}. The site distributions are given for $\theta_{Xe} < 0.33$, the coverage above which the Xe adsorption energetics are dominated by repulsive Xe-Xe interactions, rather than adsorption site structure. The fractional site occupations have been scaled such that they sum to 1.0 at $\theta_{Xe} = 0.33$. For the Pt(531) surface we have not included the PAX estimates for Xe adsorption on terrace sites because it is only a very small fraction of the total and because the overlap of the Xe $5p_{3/2}$ PAX signal from kink sites probably results in a poor estimate of Xe $5p_{1/2}$ PAX signal from the terraces (Fig. 5).

4.2. Quantification of adsorption site distributions from Xe TPD

On the Pt surfaces the Xe adsorption site occupancy can also be estimated from the TPD spectra shown in Fig. 2. This was not possible on the Cu surfaces which yielded very weakly structure sensitive Xe TPD spectra [15]. On the Pt(111) surface there is a distinct feature at 92 K in the high coverage Xe TPD spectra that has been associated with the formation of an ordered $(\sqrt{3} \times \sqrt{3})R30$ structure as the Xe coverage during heating decreases to $\theta_{Xe} < 0.33$ [29]. At higher coverages, the overlayer structure is incommensurate with the Pt(111) substrate and there are strong repulsive lateral interactions that decrease the effective adsorption energy of Xe resulting in desorption at T < 92 K. The integrated area from 92 to 160 K on the Pt(111) surface corresponds to a coverage of $\theta_{Xe} = 0.33$ Xe/Pt. The integrated area from 92 to 160 K has also been used to define $\theta_{Xe} = 0.33$ on the Pt(221) and Pt(531) surfaces,

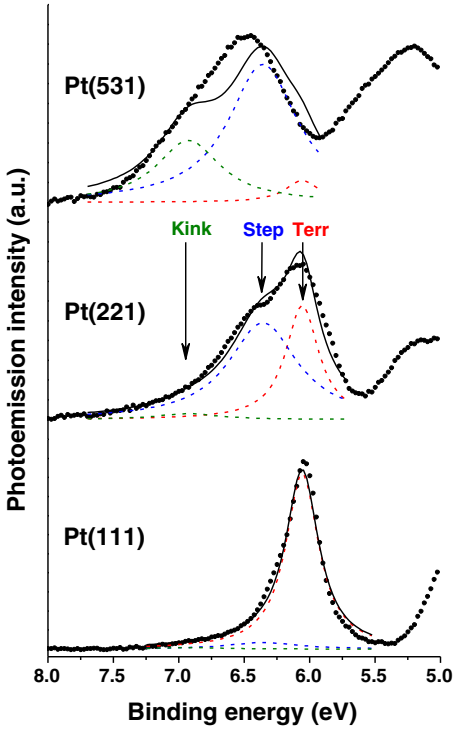

Fig. 5. Fits of the PAX spectra at saturation Xe coverage on Pt(111), Pt(221) and Pt(531) surfaces using the peak parameters in Table 1. The symbols are baseline subtracted data points and the solid lines are the spectral fits. The terrace, step and kink components of each total fit are shown in the dashed lines.

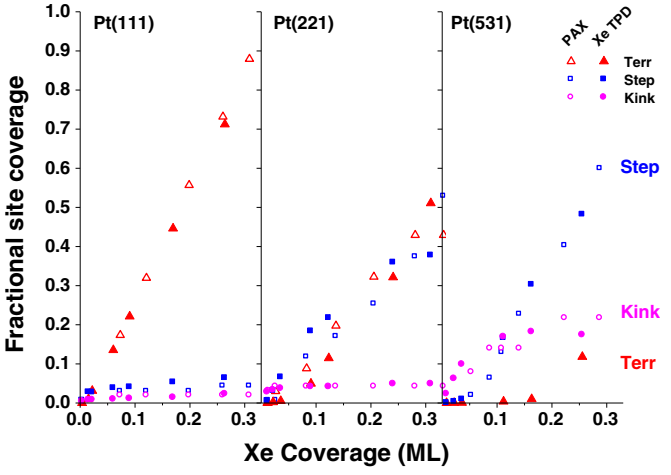

Fig. 6. Xe coverage on terrace, step and kink sites versus total θ_{Xe} determined from analysis of the PAX spectra. The open symbols (Δ—terrace, □—step, ○—kink) were obtained from the fit of the PAX spectra using the parameters in Table 1. The filled symbols (▲—terrace, ■—step, ●—kink) were obtained from the areas of the Xe TPD peaks.

although referencing this coverage to the number of surface Pt atoms is no longer meaningful.

The Xe TPD spectra from Pt(111) show that for initial coverages up to $\theta_{Xe} = 0.33$ Xe/Pt desorption of Xe from the terraces occurs over the temperature range 92–105 K. The high temperature desorption feature is associated with Xe desorption from the residual steps in the Pt(111) surface. The dominant desorption feature from the Pt(221) surface at initial coverages similar to the $\theta_{Xe} = 0.33$ on the Pt(111) occurs over the temperature range 90–125 K. We assume that this is associated with desorption from the step edges and from the terraces on Pt(221). The higher temperature feature observed at very low θ_{Xe} is associated with desorption from residual kinks in the step edges. Finally, desorption from the Pt(531) surface at a Xe coverage similar to the $\theta_{Xe} = 0.33$ observed on Pt(111) occurs over the temperature range 90–150 K. The Xe adsorption sites on the three different Pt surfaces have been estimated from the TPD spectra by integrating the desorption features from each spectrum in Fig. 2 over the temperature ranges 92–105 K, 105–125 K, and 125–160 K to estimate the fraction of Xe atoms desorbing from terrace, steps and kink sites, respectively. The fractional site coverages versus θ_{Xe} as determined from the Xe TPD experiments are compared with the results of the PAX analysis by the filled symbols in Fig. 6. The fractional site occupations have been scaled such that they sum to 1.0 at $\theta_{Xe} = 0.33$. For $\theta_{Xe} > 0.33$ the desorption energetics are dominated by repulsive interatomic interactions rather than the structural nature of the adsorption site.

4.3. Xe adsorption site distributions on Pt(111), Pt(221) and Pt(531)

Both PAX and Xe TPD have been used to provide complementary estimates of the adsorption site distributions and their fractional occupation by Xe as it is adsorbed at increasing coverages on the Pt(111), Pt(221) and Pt(531) surfaces. Fig. 6 displays the fractional population of the terrace, step and kink sites versus θ_{Xe}. Not surprisingly, the PAX and Xe TPD results on the Pt(111) surface are entirely consistent with one another. Both indicate some initial adsorption at step edges and kinks. These sites arise from a combination of Pt(111) crystal misorientation, and thermal roughening and are saturated with Xe at low coverages. Both the Xe TPD and PAX data indicate that the steps represent 2–3% of the Xe adsorption sites and the kinks represent <1% of the Xe adsorption sites on the Pt(111) surface. Bear in mind that the densities of these step and kink sites are ~1% and <0.5%, respectively, relative to the Pt atom density. As the Xe coverage is increased past $\theta_{Xe} = 0.03$, the additional Xe is adsorbed exclusively at the terrace sites until the Xe coverage reaches $\theta_{Xe} = 0.41$.

The adsorption of Xe on the Pt(221) clearly reveals the presence of steps. At $\theta_{Xe} < 0.03$ ML the Xe is preferentially adsorbed at kinks in the existing step edges. The total kink site density based on both PAX and Xe TPD is ~0.03 ML (relative to the areal density of Pt atoms in Pt(111)). At Xe coverages in the range $\theta_{Xe} = 0.1$–0.33, both the steps and the terrace sites are filled, with roughly equal probability. This is interesting given that the Xe TPD experiments suggest that there should be a small energetic preference for adsorption at the step edges. Using the Redhead analysis and a pre-exponential factor of 10^{13} s^{-1} for the pre-exponential factor, one would estimate that the adsorption energy at the (110) step edges is ~4 kJ/mole higher than on the (111) terraces.

STM images of the Pt(332) surface reveal a periodic array of straight step edges and no evidence of thermal roughening (over the ~10 × 10 nm^2 area shown) [37]. The Pt(332) surface has (111) terraces that are roughly twice as wide as those on Pt(221), but also separated by (110) step edges. The Pt(332) STM image is consistent with the PAX data and Xe TPD data for Pt(221) in that the terraces on Pt(221) are wide enough only for two rows of adsorbed Xe, one at the step edge and one on the terrace, and show evidence for only a very low density of kink sites.

The ideal structure of the Pt(531) surface (Fig. 1) could be described as being formed entirely of kinks in the sense that the three low Miller index microfacets forming the surface are each only one unit cell wide. Both the PAX and the Xe TPD clearly reflect a real surface structure that is dominated by both steps and kinks. The PAX data are probably not quantitatively useful for estimation of the terrace site density because of the overlap of the high binding energy tail of the Xe $5p_{3/2}$ feature with the low binding energy side of the Xe $5p_{1/2}$ feature that has been used for determination of terrace site occupation. The apparent contribution of terrace sites to the PAX spectra is ~5%, however, the data has not been included in Fig. 6 because it is probably not meaningful. Furthermore, the Xe TPD data indicate that at low Xe coverages there is no adsorption at terrace sites. At a coverage of $\theta_{Xe} = 0.3$ there is indication of ~8% terrace sites. Both the PAX and the Xe TPD data indicate the presence of a high density of both kink and step adsorption sites. At low coverage, the kinks sites are populated first; however, as the coverage increases the fraction of step sites exceeds that of the kink sites. As θ_{Xe} approaches 0.33 the PAX and Xe TPD spectra both suggest a distribution of 3:1 step to kink sites. These clearly indicate that thermal roughening has reduced the kink density well below that of the ideal surface structure.

Although there are no published STM images of the Pt(531) surface, its structure has been studied by LEED and Density Functional Theory (DFT) [16,17]. LEED provides clear evidence of extensive thermal roughening resulting in cancelation of diffraction intensities over wide ranges of electron energy. DFT suggests that on a highly corrugated surface such as (531), there is little energy penalty to further roughening. The only existing images of an FCC(531) surface have been obtained from Cu(531) [38]. These reveal the high degree of thermal roughening that is also certainly present on the Pt(531) surface. These data are consistent with the PAX and Xe TPD results of our work. Roughening of the Pt(531) surface must involve motion of atoms that reduces the kink density and results in the formation of sites that are step-like, even if the steps only extend over two to three atomic spacings. The PAX and Xe TPD data from Pt(531) suggest that the fraction of sites that are step-like is almost twice the fraction of kink-like Xe adsorption sites. Consistent with the STM image of Cu(531), roughening of the Pt(531) surface is not sufficient to create a large fraction of terrace sites.

5. Conclusions

A complementary combination of PAX and Xe TPD measurements on the Pt(111), Pt(221) and Pt(531) surfaces has provided a quantitative description of the distribution of terraces, step and kink sites exposed by these surfaces for Xe adsorption at coverages up to $\theta_{Xe} = 0.33$ relative to the density of Pt atoms in the Pt(111) surface. The Pt(111) surface exposes ~95% terraces sites, as expected. The sites measured by Xe adsorption on Pt(221) have a roughly equal fraction of terrace and step edge sites that are occupied with roughly equal probability as the coverage increases from $\theta_{Xe} = 0.05$ to 0.33. PAX and Xe TPD reveal the presence of kink sites on the Pt(531) surface; however, thermal roughening reduces the fraction of kink sites to roughly 25% of the total with the majority being step sites. On the Pt(531) surface there is evidence of sequential filling of the kink, step and terraces sites, in that order, as the Xe coverage increases.

Acknowledgments

LB acknowledges support of the NSF under grant no. CHE-1012358 for collection of the experimental data reported herein. BH acknowledges support by the US Department of Energy under grant no. DE-FG02-12ER16330 for analysis of the data.

References

[1] C.F. McFadden, P.S. Cremer, A.J. Gellman, Langmuir 12 (1996) 2483.
[2] G.A. Attard, A. Ahmadi, J. Feliu, A. Rodes, E. Herrero, S. Blais, G. Jerkiewicz, J. Phys. Chem. B 103 (1999) 1381.
[3] A. Ahmadi, G. Attard, J. Feliu, A. Rodes, Langmuir 15 (1999) 2420.

[4] T.D. Power, D.S. Sholl, Top. Catal. 18 (2002) 201.
[5] T.D. Power, A. Asthagiri, D.S. Sholl, Langmuir 18 (2002) 3737.
[6] A. Asthagiri, P.J. Feibelman, D.S. Sholl, Top. Catal. 18 (2002) 193.
[7] A.E. Baber, A.J. Gellman, D.S. Sholl, E.C.H. Sykes, J. Phys. Chem. C 112 (2008) 11086.
[8] D.S. Sholl, A. Asthagiri, T.D. Power, J. Phys. Chem. B 105 (2001) 4771.
[9] T.D. Power, D.S. Sholl, J. Vac. Sci. Technol. A 17 (1999) 1700.
[10] D.S. Sholl, Langmuir 14 (1998) 862.
[11] Y. Huang, A.J. Gellman, Top. Catal. 54 (2011) 1403.
[12] Y. Huang, A.J. Gellman, Catal. Lett. 125 (2008) 177.
[13] J.D. Horvath, A. Koritnik, P. Kamakoti, D.S. Sholl, A.J. Gellman, J. Am. Chem. Soc. 126 (2004) 14988.
[14] J.D. Horvath, A.J. Gellman, J. Am. Chem. Soc. 124 (2002) 2384.
[15] L. Baker, B. Holsclaw, A.E. Baber, H.L. Tierney, E.C.H. Sykes, A.J. Gellman, J. Phys. Chem. C 114 (2010) 18566.
[16] S.R. Puisto, G. Held, V. Ranea, S.J. Jenkins, E.E. Mola, A.A. King, J. Phys. Chem. B 109 (2005) 22456.
[17] S.R. Puisto, G. Held, D.A. King, Phys. Rev. Lett. 95 (2005) 036102.
[18] A. Jablonski, K. Wandelt, Surf. Sci. 251 (1991) 650.
[19] A. Jablonski, K. Wandelt, Surf. Interface Anal. 17 (1991) 611.
[20] K. Wandelt, Springer Ser. Surf. Sci. 22 (1990) 289.
[21] R.D. Boutchko, L.W. Bruch, Phys. Rev. B 70 (2004).
[22] F. Brunet, R. Schaub, S. Fedrigo, R. Monot, J. Buttet, W. Harbich, Surf. Sci. 512 (2002) 201.
[23] S. Horch, P. Zeppenfeld, G. Comsa, Appl. Phys. Mater. Sci. Process. 60 (1995) 147.
[24] B. Lehner, M. Hohage, P. Zeppenfeld, Phys. Rev. B 65 (2002).
[25] C.T. Rettner, D.S. Bethune, E.K. Schweizer, J. Chem. Phys. 92 (1990) 1442.
[26] T. Seyller, M. Caragiu, R.D. Diehl, P. Kaukasoina, M. Lindroos, Phys. Rev. B 60 (1999) 11084.
[27] H.R. Siddiqui, P.J. Chen, X. Guo, J.T. Yates, J. Chem. Phys. 92 (1990) 7690.
[28] P.S. Weiss, D.M. Eigler, Phys. Rev. Lett. 69 (1992) 2240.
[29] W. Widdra, P. Trischberger, W. Friess, D. Menzel, S.H. Payne, H.J. Kreuzer, Phys. Rev. B 57 (1998) 4111.
[30] P. Zeppenfeld, S. Horch, G. Comsa, Phys. Rev. Lett. 73 (1994) 1259.
[31] S. Daiser, K. Wandelt, Surf. Sci. 128 (1983) L213.
[32] B. Cathrine, D. Fargues, M. Alnot, J.J. Ehrhardt, Surf. Sci. 259 (1991) 162.
[33] V. Pouthier, C. Ramseyer, C. Girardet, K. Kuhnke, V. Marsico, M. Blanc, R. Schuster, K. Kern, Phys. Rev. B 56 (1997) 4211.
[34] V. Pouthier, C. Ramseyer, C. Girardet, Surf. Sci. 400 (1998) 176.
[35] O. Sneh, S.M. George, J. Chem. Phys. 101 (1994) 3287.
[36] W. Widdra, P. Trischberger, J. Henk, Phys. Rev. B 60 (1999) R5161.
[37] E.A. Carbonio, M.J. Prieto, A. de Siervo, R. Landers, J. Phys. Chem. C 118 (2014) 28679.
[38] M.L. Clegg, S.M. Driver, M. Blanco-Rey, D.A. King, J. Phys. Chem. C 114 (2010) 4114.